DFT Study on the Catalytic Reactivity of a Functional Model Complex for Intradiol-Cleaving Dioxygenases

Valentin Georgiev,* Holger Noack, Tomasz Borowski, Margareta R. A. Blomberg, and Per E. M. Siegbahn

Department of Physics, Albanova, and Department of Biochemistry and Biophysics, Arrhenius Laboratories, Stockholm University, S-106 91, Stockholm, Sweden

Received: November 25, 2009; Revised Manuscript Received: March 11, 2010

The enzymatic ring cleavage of catechol derivatives is catalyzed by two groups of dioxygenases: extradiol- and intradiol-cleaving dioxygenases. Although having different oxidation state of their nonheme iron sites and different ligand coordinations, both groups of enzymes involve a common peroxy intermediate in their catalytic cycles. The factors that lead to either extradiol cleavage resulting in 2-hydroxymuconaldehyde or intradiol cleavage resulting in muconic acid are not fully understood. Well-characterized model compounds that mimic the functionality of these enzymes offer a basis for direct comparison to theoretical results. In this study the mechanism of a biomimetic iron complex is investigated with density functional theory (DFT). This complex catalyzes the ring opening of catecholate with exclusive formation of the intradiol cleaved product. Several spin states are possible for the transition metal system, with the quartet state found to be of main importance during the reaction course. The mechanism investigated provides an explanation for the observed selectivity of the complex. First, a bridging peroxide is formed, which decomposes to an alkoxy radical by O−O homolysis. In contrast to the subsequent barrier-free intradiol C−C bond cleavage, the extradiol pathway proceeds via the formation of an epoxide, which requires an additional activation barrier.

1. Introduction

Two different groups of enzymes are involved in ring cleavage of catechol derivatives: the extradiol- and intradiol-cleaving dioxygenases. Both these groups play important roles in microbial aerobic degradation of catechol derivatives and are thus important in bacterial degradation pathways.[1]

Extradiol dioxygenases contain nonheme Fe^{2+} coordinated in square bipyramidal geometry by a 2-His-1-carboxylate facial triad[2] and solvent molecules. In this coordination iron is exposed to a weak ligand field that leads to a high-spin quintet ground state. The substrates are derivatives of catechol (1,2-dihydroxybenzene) that bind directly to the iron by replacing the solvent molecules. In the first step of the catalytic cycle the substrate binds as a monoanion, causing a change in the ligation of the iron (step 1 in Figure 1), so that dioxygen can bind to iron (step 2 in Figure 1). The oxygen binding leads to a partial oxidation of the substrate, which gains cationic radical character, and dioxygen is reduced to a superoxide. An alkyl peroxide species is formed during the further course of the reaction.[3,4] Protonation of this species leads to O−O bond cleavage and the insertion of one oxygen into the catechol ring[5] (step 3 in Figure 1). Finally, hydrolysis of the lactone intermediate by the remaining hydroxide results in product release (step 4 in Figure 1).

Intradiol dioxygenases cleave the ring between the two adjacent hydroxyl substituents and utilize Fe^{3+} in their active site. Here the iron is coordinated by two histidines, two tyrosines, and a hydroxide. The catechol binds in a dianionic manner, where deprotonation of the two alcohol oxygens is facilitated by first-shell ligands (step 1 in Figure 1). Ketonization of the substrate has been suggested to provide the possibility of a direct attack of dioxygen on the substrate. However, computational results indicate that such a direct attack of triplet dioxygen on the substrate is unlikely due to a too-high activation energy.[5,6] The substrate is one-electron-oxidized, which leads to an Fe^{2+}−semiquinone species. This intermediate then binds dioxygen to the metal, and a subsequent attack on the ring leads to the bridging peroxide (step 2 in Figure 1). The incorporation of the first oxygen atom into the ring proceeds via a so-called Criegee rearrangement, which is a concerted O−O bond heterolysis and O−C attack leading to C−C bond cleavage and insertion of the attacking oxygen into the ring (step 3 in Figure 1). This step is facilitated by HOX coordination (water molecule or a first-shell ligand) that leads to protonation of the remaining oxygen. Nucleophilic attack of the newly formed hydroxide then yields the final product, *cic*,*cis*-muconic acid (step 4 in Figure 1).

It should be noted that the present description, obtained from calculations for both extradiol and intradiol mechanisms, involves a homolytic cleavage of the O−O bond.[5,7−9] In one case, for the intradiol dioxygenase 3,4-PCD a heterolytic Criegee rearrangement was also obtained.[9] The energetic difference of 2.2 kcal/mol between the homolytic and the heterolytic cleavage, however, is not sufficient for concluding which one is more favorable. Based on experiments, Bugg et al.[10] suggest that the extradiol cleavage is heterolytic, while the intradiol one is homolytic. However, this difference is not possible to resolve by experiments as long as no intermediate has been detected. From the present calculations an intermediate with a sufficiently long lifetime appears very unlikely.

Although much is known about each class of enzymes, the factors that determine intra- versus extradiol specificity are still under debate. Accurate biomimetic models can provide valuable insights to the discussion. The enzymes utilize an ordered mechanism, with substrate binding prior to dioxygen binding. Thus, isolated iron−catecholato complexes, such as the one

* Corresponding author. Telephone: +46 8 161268. Fax: +46 8 55378601. E-mail: valyo@physto.se.

10.1021/jp911217j
Published on Web 04/13/2010

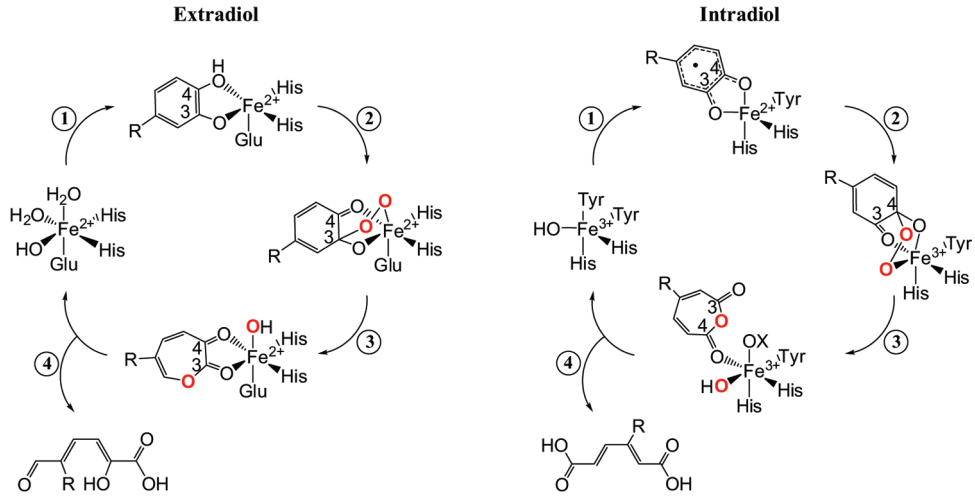

Figure 1. Proposed catalytic cycles for extra- and intradiol-cleaving dioxygenases.

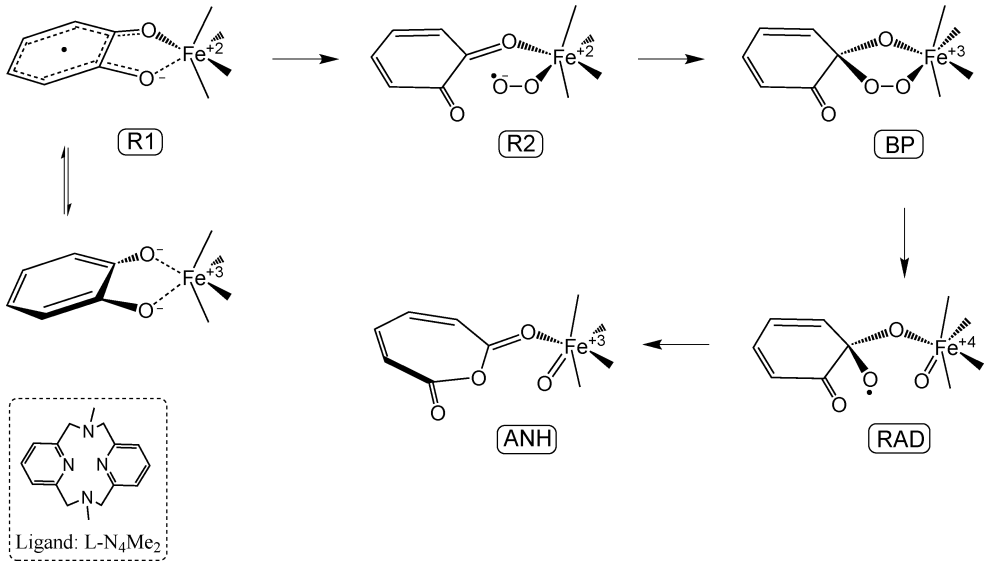

Figure 2. Proposed mechanism for intradiol cleavage catalyzed by the iron(III)L-N_4Me_2 complex (L-N_4Me_2 = *N*,*N*′-dimethyl-2,11-diaza[3.3](2,6)pyridinophane) based on the calculations.

investigated here, serve as good starting points for modeling studies. In a study on biomimetic iron compounds with a series of different ligands, it was found that the reactivity of the complex correlates with the Lewis acidity of the iron(III) center.[11] Another model complex has been reported to mimic the coordination environment found in the enzymes, having a chelating ligand providing two nitrogen and one oxygen donors. However, this complex was found to have no product specificity.[12] The functional model complex investigated here has a rather rigid ligand that provides four nitrogen donors. It can activate dioxygen at room temperature to oxidize catechol exclusively to mucon acid anhydride with a turnover number of 54.[13] The proposed mechanism based on our calculations is given in Figure 2.

Iron is coordinated by a tetraazamacrocyclic ligand L-N_4Me_2, having thus two adjacent coordination sites available for the binding of the substrate (**R1**). Binding of dioxygen, however, requires partial dissociation of the substrate to provide a free coordination site. With oxygen binding to the iron, the substrate is oxidized to a diketone (**R2**). In the next step the superoxide attacks the substrate and forms a bridging peroxide (**BP**). Finally, the O−O bond is cleaved homolytically, resulting in a radical state (**RAD**) which decays into the intradiol product (**ANH**). The experimentally determined velocity constants for the substrate catechol and di-*tert*-butyl catechol are 2.77×10^{-3} and 3.77×10^{-1} M^{-1} s^{-1}, respectively.[13] This corresponds to activation barriers of 21.0 and 18.0 kcal/mol, which might be compared to the rate constant for intradiol-cleaving catechol dioxygenase[14] with $k = 2.5 \times 10^5$ M^{-1} s^{-1} (corresponding to a barrier of 10.1 kcal/mol). Even though the coordination environments of the functional model complex and the enzyme are quite different, questions regarding the C−C cleavage step, the actual attack of the dioxygen molecule on the iron(III)−catechol system, and the intradiol specificity can be addressed.

2. Computational Details

The computational model used in this work is based on the crystal structure reported for the catecholate complex $[(LN_4Me_2)Fe(II)(cat)^-]^+$ [13] (denoted as **R1**). The calculations were done using the hybrid density functionals B3LYP[15−19] and B3LYP*, for which the amount of Hartree−Fock exchange is reduced from 20% to 15%.[20] This has been found to work better for transition metal containing systems.[21] In this study the rate-limiting step was lowered by 5.4 kcal/mol when B3LYP* was used instead of B3LYP.

Geometry optimizations were done with the software package Jaguar 5.5,[22] using the B3LYP functional with the lacvp basis set, which is composed of the 6-31G description for all light atoms and an effective core potential (ECP) on iron.[23] The final energies for the fully optimized structures were calculated with both B3LYP and B3LYP* functionals and the cc-pVTZ(-f) basis set. This intrinsically polarized triple-ζ basis set does not include an ECP; therefore the lacv3p basis set was explicitly used for iron. Experience has shown that geometries obtained from calculations using the double-ζ basis are quite adequate for the calculation of the final energetics.[24,25] Unless stated otherwise, only the B3LYP* results are reported below.

Hessian matrices (i.e., matrices of force constants) were calculated with B3LYP/lacvp, using Gaussian 03.[26] The calculation of the Hessians was necessary to find and verify transition states. Furthermore, the Hessian is needed to evaluate zero point effects, entropic and thermal corrections to the Gibbs free energy for each stationary point. The calculated entropic contribution for the oxygen binding is 8.6 kcal/mol, which goes up to 13.4 kcal/mol during the formation of the bridging peroxide. Once dioxygen is bound, and the reaction has started, the relative entropy effects vary by 0−2 kcal/mol. To account for compensating effects in the oxygen binding, a van der Waals correction was evaluated with B3LYP-D using the Orca Package.[27,28] Corrections of 3−4 kcal/mol were calculated for these long-range dispersion interactions.

To reproduce the polarization effects of the solvent used in the experiments, the self-consistent reaction field (SCRF) method implemented in Jaguar 5.5 was employed.[29,30] The solvent was modeled as a macroscopic continuum with a dielectric constant of 36.6 (corresponding to acetonitrile), and the solute was placed in a cavity contained in this continuous medium. Final energies of the optimized structures were corrected for the solvent effects by employing the lacvp basis set. In general, the dielectric medium should have a small effect on the reaction energetics as long as no substantial charge separations are involved.[31,32] However, some internal charge separation is present in this case and solvent effects therefore range from 4 to 10 kcal/mol. Reported spin populations are used to indicate the spin and oxidation states of the metal ion and were derived from a Mulliken population analysis.

3. Results and Discussion

Electronic Ground State of the Reactant. The open-shell nature of the transition metal leads to several possible spin states of the system. In order to explore the reaction coordinate, one needs to know the energetic splitting of these states for all the reaction intermediates. The iron(III) containing reactant complex can have three different spin states: sextet (spin 5/2), quartet (spin 3/2), and doublet (spin 1/2). Due to possible reduction of the iron by the substrate, a total number of eight spin states exist for **R1**. This number originates from various couplings between the unpaired electrons arising upon one-electron transfer from the substrate to iron. However, some of these states were found to be energetically high and thus thermally inaccessible and will not be considered in the discussion. A summary of the calculated relative energies for the lowest spin states for the reactant is given in Table 1.

TABLE 1: Calculated Spin Splittings in the Reactant R1 Using the B3LYP* Functional[a]

S	oxid state	Fe	catechol	Δ*G*
1/2	Fe(II)	−	1α	0.0 (3.8)
3/2	Fe(II)	2α	1α	0.8 (3.3)
	Fe(II)	4α	1*β*	4.5 (1.5)
	Fe(III)	3α	−	8.8 (10.8)
5/2	Fe(II)	4α	1α	1.2 (0.0)

[a] Relative free energies given in kcal/mol. Values in parentheses are obtained with the B3LYP functional.

From experiments this complex is predicted to be high spin ($S = 5/2$) based on the typical bond lengths commonly observed in high-spin complexes with this ligand.[13] The ground state of the reactant predicted by the calculations differs depending on the functional used. For B3LYP the calculations agree with experiments, finding ^{6}[**R1**]$_{4\alpha1\alpha}$ as the ground state, i.e., $[(LN_4Me_2)Fe(II)(cat)^-]^+$. If the amount of exact Hartree−Fock exchange is lowered to 15%, low-spin states are slightly preferred, and the experimental ground state goes up to 1.2 kcal/mol. However, it can be seen that the different spin states are very close in energy and the B3LYP* functional will be used in the following since it has been shown to provide reliable energies for systems involving transition metals.[21] The calculated Fe−N_{py} and Fe−N_{amine} distances of 2.13 and 2.32 Å, as well as the N_{py}−Fe−N_{amine} angle of 147°, are in reasonably good agreement with experiments. Finally, a reactant state involving Fe(III) and unoxidized substrate was found to be high for both functionals and is thus unlikely to be involved in the reaction.

The dominating ferrous−semiquinonate resonance is very important for the next catalytic step, as it directs the dioxygen

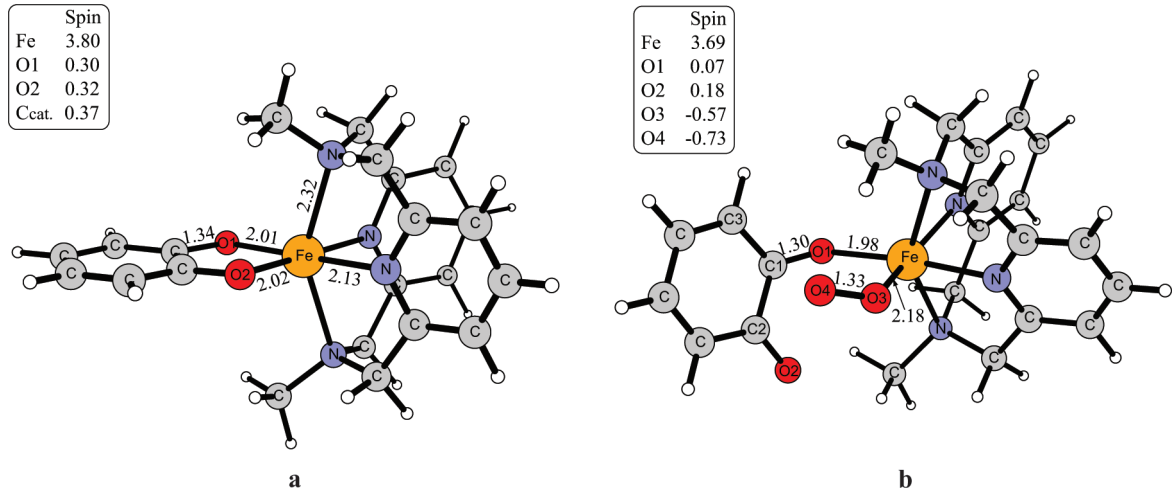

a **b**

Figure 3. (a) Reactant ^{6}**R1** in its high-spin ground state (4α1α); (b) superoxide complex ^{4}**R2**.

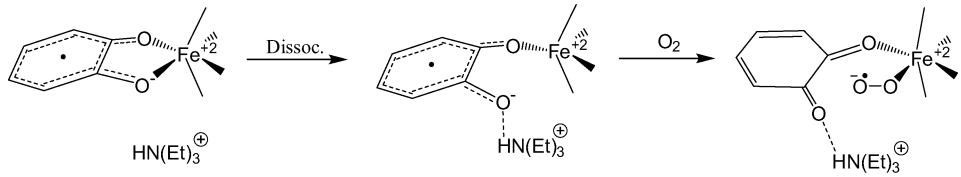

Figure 4. Dissociation of one catecholate bond to provide a coordination site for dioxygen is supported by triethylamine.

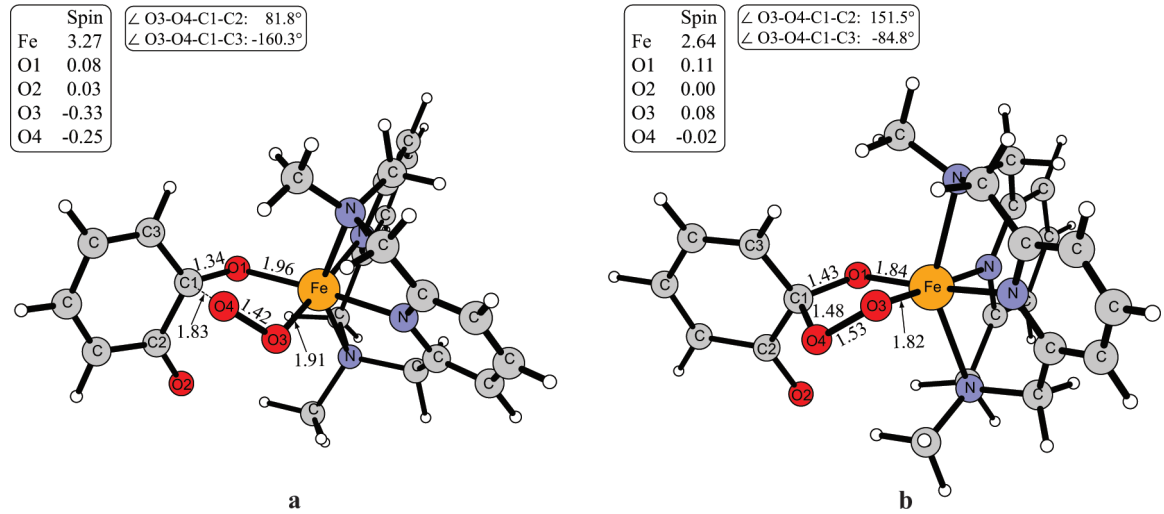

Figure 5. (a) Transition state for peroxide formation ^{4}**TS1**; (b) bridging peroxide ^{4}**BP**.

binding directly to the metal. In this respect the computational results for the biomimetic model complex considered here are in line with previous theoretical[6,9] and experimental[33] findings concerning intradiol cleavage in enzymes.

Dioxygen Binding. The formation of the oxygen adduct **R2** from **R1** and $^3O_2$ is accompanied by one-electron reduction of the dioxygen molecule to a superoxide O_2^-. The electron is provided by the substrate radical, which in turn becomes a neutral quinone. One oxygen atom of the substrate must dissociate from the metal ion upon oxygen binding to provide the necessary coordination site; see Figure 3b.

Two spin states for the **R2** complex with quite close energies were identified—a quartet ^{4}[**R2**]$_{4\alpha1\beta}$ and a sextet ^{6}[**R2**]$_{4\alpha1\alpha}$—where the unpaired electrons are residing on iron and oxygen, respectively (no spin on the substrate). The quartet state lies at 18.0 kcal/mol and the sextet state at 18.2 kcal/mol relative to the reaction zero level. Additionally, a doublet state ^{2}[**R2**]$_{1\alpha}$ exists at an energy level of 26.6 kcal/mol.

The relatively high energies of the oxygen adduct is mainly due to energy required to dissociate one of the substrate oxygens from iron. In the absence of dioxygen this dissociation cannot be achieved without applying a geometry constraint on the oxygen−iron distance during the optimization. The oxygen binding was therefore investigated by using a test model including a protonated triethylamine ($[NH(Et)_3]^+$), as $N(Et)_3$ is a base present in the experimental setup.[13] Upon coordination of the $[NH(Et)_3]^+$ to one of the oxygens of the substrate, the dissociation becomes an accessible minimum with an energy of 13.0 kcal/mol. Subsequent oxygen binding then only requires 3.7 kcal/mol free energy; see Figure 4.

Thus, in total oxygen binding requires an activation barrier of 16.7 kcal/mol in the presence of the base. This shows that most of the energy needed to form the oxygen-bound adduct ^{4}[**R2**]$_{4\alpha1\beta}$ is due to the dissociation of the semiquinonate. Since the total O_2 binding energy given by the test model was essentially the same as without the base, the investigation was continued with the initial model. The possibility of direct dioxygen binding to the substrate instead of the metal was also investigated. However, it was not possible to obtain such a complex without constraining the distance between a catecholate carbon atom and O_2. Furthermore, these computational model complexes were found to be 8−12 kcal/mol higher than the corresponding metal-bound structures; hence it can be concluded that direct oxygen binding to the substrate is unlikely to occur. These results are in good agreement with the predominant ferrous character that was found in the **R1** complex, which enables direct binding of the dioxygen to the metal.

O−O Bond Cleavage. From the **R2** complex the reaction proceeds via an attack of the superoxide on the aromatic ring of the substrate. The second electron required for the reduction of the superoxide to a peroxide is provided by iron(II), which is thus oxidized to Fe(III). The transition state ^{4}**TS1** (Figure 5a) for this step lies at 23.3 kcal/mol on the quartet surface. No corresponding transition state was found on the sextet surface; instead, a transition state was found leading to another intermediate (see below). The formation of the bridging peroxide ^{4}**BP** (Figure 5b) is slightly exergonic with a reaction free energy of −4.5 kcal/mol. The ground state for this intermediate is a quartet, with a doublet state around 10 kcal/mol higher energy. No bridging peroxide could be found on the sextet potential energy surface.

From ^{4}**BP** the reaction proceeds with a homolytic O−O bond cleavage resulting in formation of a radical state ^{4}**RAD**, an Fe(IV)−oxo species containing an alkoxy radical on the substrate. The activation free energy for the bond cleavage is 8.0 kcal/mol with respect to ^{4}**BP**. The optimized geometry for the transition state, ^{4}**TS2**, is shown in Figure 6a, and the spin population on both oxygen atoms originating from the O_2 molecule clearly indicates a homolytic bond cleavage. The calculated reaction free energy for this step is 0.6 kcal/mol, indicating that the O−O bond cleavage is close to thermoneutral.

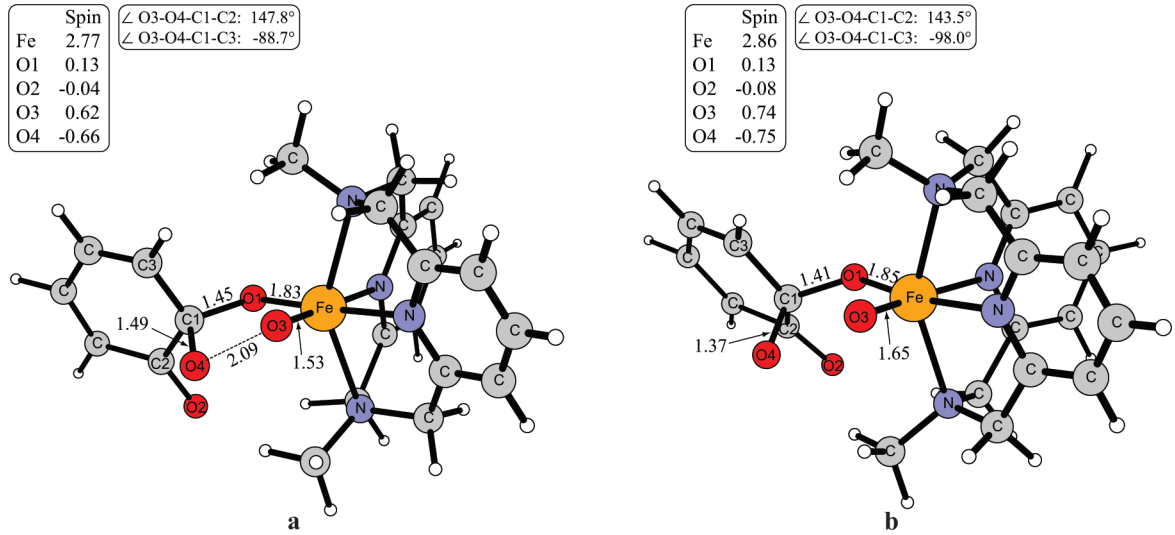

Figure 6. (a) Transition state for the homolytic O−O bond cleavage ^{4}**TS2**; (b) alkoxyl radical, ^{4}**RAD**, formed after the O−O bond cleavage.

The same kind of alkoxyl radical intermediate was also found in previous studies on extra- and intradiol dioxygenases (Fe- and Mn-dependent)[5,8,9,34] and homogentisate dioxygenase.[7] In all these cases this short-lived radical intermediate spontaneously converts into the next intermediate. Such an alkoxy radical intermediate is absent in the case of an experimentally suggested Criegee rearrangement with a heterolytic cleavage process. The Criegee rearrangement has a stringent requirement for in-plane orientation of the two oxygen atoms and the two carbon atoms involved in bond cleavage and formation.[9] Furthermore, it also necessitates the peroxo group being protonated. Since in the current system the rigid ligand on iron does not provide enough flexibility, the relevant dihedral angle (O3−O4−C1−C2 = 151.1°; see Figure 5b) is substantially off the optimal value of 180, and the peroxo group does not bear a proton, the transition state for the heterolytic Criegee rearrangement could not be found.

Notably, the existence of the radical intermediate opens the possibility for the alternative extradiol reaction. The results describing the selectivity of the ring cleavage and thus the specificity of intra- versus extradiol ring cleavage are presented in the next section.

On the sextet potential energy surface (PES) the peroxide intermediate was not found. The sextet state ^{6}**R2** undergoes a direct homolytic O−O bond cleavage leading to Fe(IV)−oxo/alkoxy radical ^{6}**RAD**. A transition state for this process was found and fully optimized, but it lies 15.3 kcal/mol above the corresponding ^{4}**TS2**. Also, the resulting alkoxy radical intermediate is 7.4 kcal/mol less stable than the equivalent quartet state structure. These energy differences clearly indicate that the quartet path, going through a peroxy intermediate, is the preferred one for the reaction.

Comparison of Intra- and Extradiol Bond Cleavage. The Fe(IV)−oxo/alkoxy radical intermediate plays a pivotal role for the intra- vs extradiol cleavage selectivity. It is therefore quite important to explore both reactions and find out which one is energetically favorable. A summary of the reaction profiles is shown in Figure 7. From ^{4}**RAD** the intradiol path proceeds in a single step involving C−C bond cleavage and C−O bond formation. The transition state ^{4}**TSi** for this intradiol cleavage could be located on the quartet PES using the small basis set, as described under Computational Details. However, the large basis set correction to the energy lowered the energetic position of that transition state below that of the radical state ^{4}**RAD**. Therefore, it can be concluded that, within the computational accuracy, the formation of the intradiol product proceeds to ^{4}**ANH** (Figure 9) with at most a small barrier.

The reaction free energy obtained for the entire reaction is −33.9 kcal/mol. The sextet product ^{6}**ANH** was calculated to be 3.2 kcal/mol more stable than the quartet, which indicates that the system undergoes an intersystem crossing back to the resting sextet spin state.

The alternative reaction leading to an extradiol cleavage product proceeds via the intermediate formation of an epoxide (**EO** if Figure 7). On the quartet surface this requires an energy of 4.1 kcal/mol to overcome the activation barrier. The corresponding transition state is shown in Figure 8b. This differentiation between the intra- and extradiol C−C bond cleavage is in good agreement with previous theoretical results. More specifically, it has been observed that if the mechanism involves a radical intermediate after the O−O bond cleavage, there is one specific carbon atom which is attacked spontaneously by the oxygen radical, whereas the attack on the other carbon involves a barrier of 3−4 kcal/mol.[5,7−9,34] The preferred reaction channel, which may lead either to *intra* or *extra* cleavage, always involves the carbon atom for which the C−C−O−O dihedral angle is closer to 180°. Indeed, as shown in Figure 6b, in the present case it is the carbon C2 which is placed in the reactive position with the C2−C1−O4−O3 dihedral amounting to 143.5°, and the attack on C2 is barrierless. This geometric preference might have its roots in the fact that the singly occupied orbital on the oxygen (O4) evolves from the σ^* O−O orbital and it remains oriented along the O−O vector even when the O−O bond is broken. Thus, the C−C−O−O dihedral angle close to 180° guarantees a good overlap of the C−C σ and singly occupied O(2p) orbital, and hence a spontaneous reaction. The attack on the other carbon requires reorienting the O(2p) orbitals so that the singly occupied orbital interacts with the target carbon whereas the doubly occupied one points toward the oxo iron ligand, and this reorientation is most likely responsible for the 3−4 kcal/mol barrier. It should be noted, however, that this preference for in-plane arrangement of the C−C and O−O vectors is much less strict than for the heterolytic Criegee rearrangement because in the radical process the O−O bond breaking and the attack on the carbon are sequential, whereas in the heterolytic reaction these two steps are concerted. Hence, the dihedral angle around

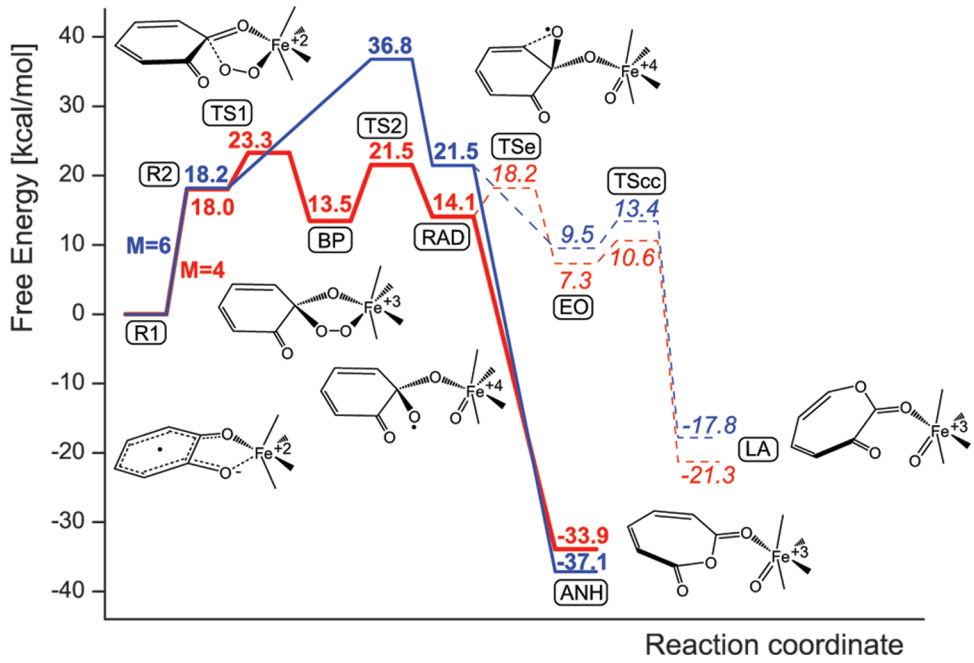

Figure 7. Calculated energy profile along the reaction coordinate (using the B3LYP* functional); red, quartet state PES; blue, sextet state PES; solid line, observed intradiol reaction path; dashed line, alternative extradiol reaction path.

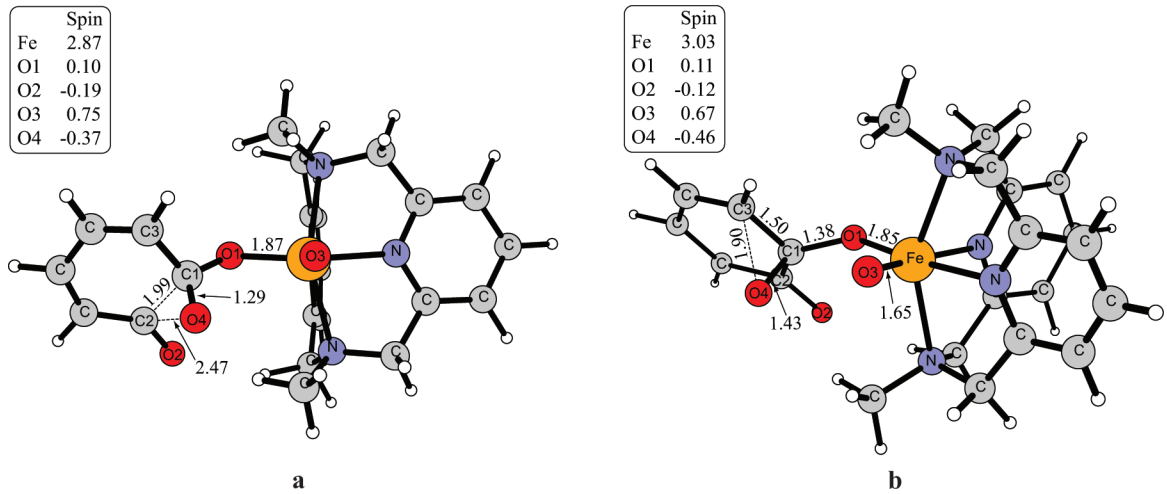

Figure 8. (a) Transition state for intradiol cleavage ^{4}**TSi**; (b) transition state for epoxide formation ^{4}**TSe**.

140° determines the chemoselectivity of the radical process, yet it deviates too much for a heterolytic Criegee rearrangement.

For the sextet surface the barrier for the extradiol path disappears when applying the big basis set correction, but this path is still higher in energy than the intradiol one. The C−C bond cleavage **TScc** after the epoxide formation on the extradiol path requires an activation barrier of +3.3 kcal/mol. The resulting extradiol cleaved product **LA** has an energy of −21.3 kcal/mol for the quartet state and −17.8 for the sextet state. Thus, the observed selectivity of the reaction catalyzed by the investigated functional model complex is due to the fact that from the radical intermediate the intradiol reaction proceeds with essentially no barrier and is irreversible with an exergonicity of −37.1 kcal/mol, whereas the extradiol reaction goes through a barrier of 4.1 kcal/mol, leading to less stable products.

Comparison with the Enzymatic Mechanism. It is worth comparing the catalytic reaction of the present biomimetic complex with the computational results for an intradiol dioxygenase enzyme, protocatechuate 3,4-dioxygenase (3,4-PCD).[9] The mechanisms are very similar, involving essentially the same main chemical steps. Formation of a bridging peroxo intermediate after binding and one-electron reduction of the dioxygen and cleavage of the O−O bond followed by insertion of the oxygen atom into the ring are the key features of the intradiol aromatic ring cleavage. The calculated rate-limiting step for the synthetic complex is the bridging peroxide formation, with an activation barrier of 23.3 kcal/mol (for the quartet spin state), while for the enzymatic case it is the O−O bond breaking that determines the overall reaction rate with an activation barrier of 20.8 kcal/mol. The formation of the Fe(II)−$(O_2)^{\bullet-}$ adduct appears to be quite endergonic for the biomimetic complex. The reason is that the binding of the O_2 molecule requires dissociation of one of the substrate oxygens from iron, and opening of a free coordination site. Within the present model this transformation was found to be very expensive in terms of free energy. The enzymatic environment, on the other hand, provides a coordination site for dioxygen in the beginning of the reaction, and facilitates later conformational changes by stabilizing interactions with second-shell residues. For the biomimetic system, the calculated sextet spin state reaction involves too-

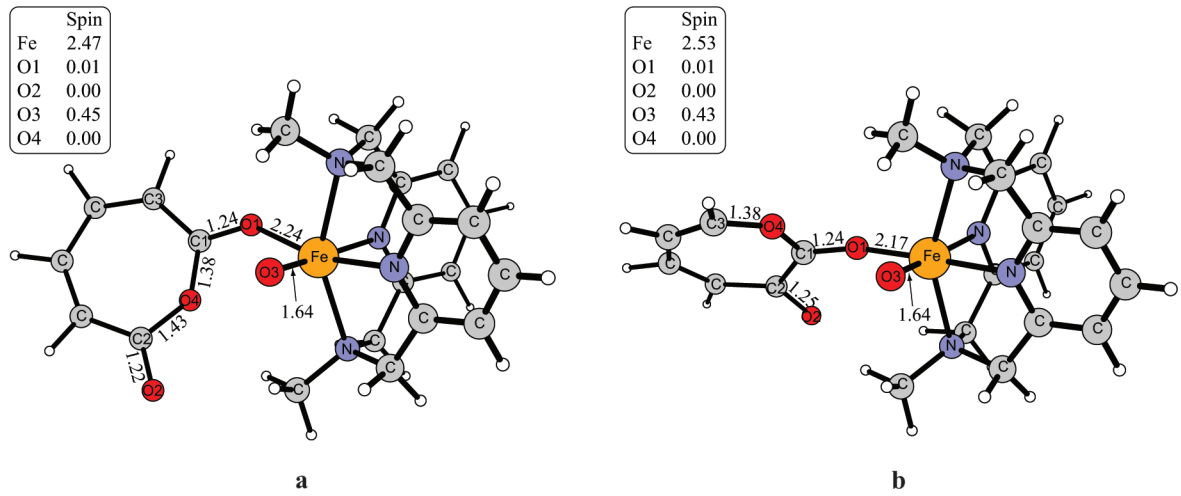

Figure 9. (a) Anhydride product of the intradiol cleavage ^{4}**ANH**; (b) lactate product of the extradiol pathway ^{4}**LA**.

TABLE 2: Comparison of the Energies (kcal/mol) Relative to the R1 Reactant for Different Spin States of Intermediates along the Reaction Coordinate[a]

intermediate	doublet	quartet	sextet
R2	26.6 (32.8)	18.0 (18.6)	18.2 (19.4)
BP	21.2 (27.7)	13.5 (18.5)	–
RAD	22.1 (30.6)	14.1 (20.7)	21.5 (27.6)

[a] Values in parentheses are calculated using the original B3LYP functional.

high energies, but spin transition to a quartet state was found to occur, where the calculated activation free energy is in good agreement with the experimentally determined one. A Criegee rearrangement transition state was found for the enzyme, which requires in-plane orientation of the two oxygen atoms and the two carbon atoms involved in bond cleavage and formation. This was not possible for the present model system, since the rigid ligand on iron does not provide enough flexibility for the proper arrangement.

4. Conclusions

A plot summarizing the theoretical results and providing a mechanism for the catalytic reaction of the biomimetic complex $[(LN_4Me_2)Fe(II)(cat)^-]^+$ is given in Figure 7. From the calculated spin splittings it can be concluded that only the quartet state is likely to be involved in an energetically plausible mechanism. The sextet, being the resting state for the reactant and the product, is involved in the beginning and the end of the reaction. Doublet states were always found to be 5−15 kcal/mol higher in energy than the corresponding quartet and sextet intermediates (Table 2).

The mechanism is summarized in Figure 2. The catecholate complex **R1** binds dioxygen and forms the adduct **R2**, in which the substrate is bound in a monodentate fashion. The dioxygen is one-electron-reduced and forms a superoxide. Attack on the aromatic ring leads to a bridging alkylperoxo complex **BP**, which is the rate-limiting step. The calculated activation free energy of 23.3 kcal/mol is in good agreement with the experimental barrier of about 21 kcal/mol. The involvement of a peroxo intermediate in both intra- and extradiol cleavage reactions is supported by a number of computational studies[5,9,10,34] and by recent experimental studies of Kovaleva et al.,[3,4] where such an intermediate was actually detected. The peroxide O−O bond cleaves homolytically to give a radical Fe(IV)−oxo intermediate **RAD**. The ring cleavage and oxygen atom insertion to give the intradiol product proceed without an activation barrier. A muconic anhydride is formed, which is the final product within the scope of the present work. The reason for this intradiol specificity can be found in the relative orientation of the substrate toward the bridging peroxide, or more precisely in the C−C−O−O dihedral. The orientation of the antibonding σ^* O−O orbital toward the target C in the bridging peroxide leads the system directly to intradiol cleavage upon homolytic cleavage of the O−O bond. The alternative path of extradiol cleavage needs to cross a small barrier of 4.1 kcal/mol mainly due to reorientation of the singly occupied O(2p) orbital. In that case the reaction leads to the formation of an intermediate epoxide, followed by C−C bond cleavage.

From these results it can be understood how second-shell histidine residues involved in the reaction in enzymes can govern the outcome of the reaction. By stabilizing or protonating the bridging peroxide, its orientation toward one of the two possible target carbons can be changed, which preselects the reaction path that follows after O−O homolysis. This is supported by the findings that the selectivity of an extradiol-cleaving enzyme was altered to intradiol cleavage upon mutation of a histidine residue involved in the reaction, or upon providing alternative substrates.[35]

References and Notes

(1) Hayaishi, O.; Katagiri, M.; Rothberg, S. *J. Am. Chem. Soc.* **1955**, *77*, 5450.
(2) Que, L., Jr. *Nat. Struct. Biol.* **2000**, *7*, 182.
(3) Kovaleva, E. D.; Lipscomb, J. D. *Science* **2007**, *316*, 453–457.
(4) Kovaleva, E. D.; Neibergall, M. B.; Chakrabarty, S.; Lipscomb, J. D. *Acc. Chem. Res.* **2007**, *40*, 475–483.
(5) Siegbahn, P. E. M.; Haeffner, F. *J. Am. Chem. Soc.* **2004**, *126*, 8919.
(6) Funabiki, T.; Yamazaki, T. *J. Mol. Catal. A* **1999**, *150*, 37.
(7) Borowski, T.; Georgiev, V.; Siegbahn, P. E. M. *J. Am. Chem. Soc.* **2005**, *127*, 17303.
(8) Georgiev, V.; Borowski, T.; Blomberg, M. R. A.; Siegbahn, P. E. M. *J. Biol. Inorg. Chem.* **2008**, *13*, 929.
(9) Borowski, T.; Siegbahn, P. E. M. *J. Am. Chem. Soc.* **2006**, *128* (39), 12941.
(10) Xin, M.; Bugg, T. D. H. *J. Am. Chem. Soc.* **2008**, *130* (31), 10423.
(11) Cox, D. D.; Que, L., Jr. *J. Am. Chem. Soc.* **1988**, *110*, 8085.
(12) Bruijnincx, P. C. A.; Lutz, M.; Spek, A. L.; Hagen, W. R.; van Koten, G.; Klein Gebbink, R. J. M. *Inorg. Chem.* **2007**, *46*, 8391.
(13) Koch, W. O.; Krüger, H.-J. *Angew. Chem., Int. Ed. Engl.* **1995**, *34*, 2671.
(14) Walsh, T. A.; Ballou, D. P.; Mayer, R.; Que, L., Jr. *J. Biol. Chem.* **1983**, *258*, 14422.
(15) Lee, C.; Yang, W.; Parr, R. G. *Phys. Rev. B* **1988**, *37*, 785.
(16) Becke, A. D. *J. Chem. Phys.* **1992**, *96*, 2155.
(17) Becke, A. D. *J. Chem. Phys.* **1992**, *97*, 9173.
(18) Becke, A. D. *J. Chem. Phys.* **1993**, *98*, 5648.

(19) Stephens, P. J.; Devlin, F. J.; Chabalowski, C. F.; Frisch, M. J. *J. Phys. Chem.* **1994**, *98*, 11623.

(20) Reiher, M.; Salomon, O.; Hess, B. A. *Theor. Chem. Acc.* **2001**, *107*, 48.

(21) Salomon, O.; Reiher, M.; Hess, B. A. *J. Chem. Phys.* **2002**, *117*, 4729.

(22) *Oregon "Jaguar 5.5"*; Schrödinger, Inc.: Portland, 2000.

(23) Hay, P. J.; Wadt, W. R. *J. Chem. Phys.* **1985**, *82*, 299.

(24) Siegbahn, P. E. M. In *Advances in Chemical Physics: New Methods in Computational Quantum Mechanics*; Prigogine, I., Rice, S. A., Eds.; John Wiley & Sons: London, 1996.

(25) *Recent advances in density functional methods, part II*; Chong, D. P., Ed.; World Scientific: Singapore, 1997.

(26) Frisch, M. J.; Trucks, G. W.; Schlegel, H. B.; Scuseria, G. E.; Robb, M. A.; Cheeseman, J. R.; Montgomery, J. A., Jr.; Vreven, T.; Kudin, K. N.; Burant, J. C.; Millam, J. M.; Iyengar, S. S.; Tomasi, J.; Barone, V.; Mennucci, B.; Cossi, M.; Scalmani, G.; Rega, N.; Petersson, G. A.; Nakatsuji, H.; Hada, M.; Ehara, M.; Toyota, K.; Fukuda, R.; Hasegawa, J.; Ishida, M.; Nakajima, T.; Honda, Y.; Kitao, O.; Nakai, H.; Klene, M.; Li, X.; Knox, J. E.; Hratchian, H. P.; Cross, J. B.; Bakken, V.; Adamo, C.; Jaramillo, J.; Gomperts, R.; Stratmann, R. E.; Yazyev, O.; Austin, A. J.; Cammi, R.; Pomelli, C.; Ochterski, J. W.; Ayala, P. Y.; Morokuma, K.; Voth, G. A.; Salvador, P.; Dannenberg, J. J.; Zakrzewski, V. G.; Dapprich, S.; Daniels, A. D.; Strain, M. C.; Farkas, O.; Malick, D. K.; Rabuck, A. D.; Raghavachari, K. Foresman, J. B.; Ortiz, J. V.; Cui, Q.; Baboul, A. G.; Clifford, S.; Cioslowski, J.; Stefanov, B. B.; Liu, G.; Liashenko, A.; Piskorz, P.; Komaromi, I.; Martin, R. L.; Fox, D. J.; Keith, T. Al-Laham, M. A.; Peng, C. Y.; Nanayakkara, A.; Challacombe, M.; Gill, P. M. W.; Johnson, B.; Chen, W.; Wong, M. W.; Gonzalez, C.; Pople, J. A. *Gaussian 03*, Revision D.01; Gaussian, Inc.: Wallingford, CT, 2004.

(27) Grimme, S. *J. Comput. Chem.* **2004**, *25*, 1463.

(28) Grimme, S. *J. Comput. Chem.* **2006**, *27*, 1787.

(29) Tannor, D. J.; Marten, B.; Murphy, R.; Friesner, R. A.; Sitkoff, D.; Nicholls, A.; Honig, B.; Ringnalda, M.; Goddard, W. A. *J. Am. Chem. Soc.* **1994**, *116*, 11875.

(30) Marten, B.; Kim, K.; Cortis, C.; Friesner, R. A.; Murphy, R. B.; Ringnalda, M. N.; Sitkoff, D.; Honig, B. *J. Phys. Chem.* **1996**, *100*, 11775.

(31) Siegbahn, P. E. M.; Blomberg, M. R. A. *Chem. Rev.* **2000**, *100*, 421.

(32) Siegbahn, P. E. M. *J. Comput. Chem.* **2001**, *22*, 1634.

(33) Costas, M.; Mehn, M. P.; Jensen, M. P.; Que, L. *Chem. Rev.* **2004**, *104*, 939.

(34) Georgiev, V.; Borowski, T.; Siegbahn, P. E. M. *J. Biol. Inorg. Chem.* **2006**, *11*, 571.

(35) Groce, S. L.; Lipscomb, J. D. *J. Am. Chem. Soc.* **2003**, *125*, 11780.

JP911217J